Regular Article

PHYSICAL CHEMISTRY RESEARCH
Published by the
Iranian Chemical Society
www.physchemres.org
info@physchemres.org

Phys. Chem. Res., *Vol. 6, No. 4, 729-740, December 2018*
DOI: 10.22036/pcr.2018.137083.1501

Graphitic Carbon Nitride/Reduced Graphene Oxide/Silver Oxide Nanostructures with Enhanced Photocatalytic Activity in Visible Light

H. Salari[a,*], A. Daliri[b] and M.R. Gholami[b,*]

[a]*Department of Chemistry, College of Sciences, Shiraz University, Shiraz, Iran*
[b]*Department of Chemistry, Sharif University of Technology, Tehran, Iran*

(Received 25 June 2017, Accepted 13 August 2018)

Visible light active graphitic carbon nitride/reduced graphene oxide/silver oxide nanocomposites with a p-n heterojunction structure were synthesized by chemical deposition methods. Prepared samples were characterized by XRD, FTIR, SEM, TEM and DRS. Photocatalytic activity investigated by analyzing the Acid blue 92 (AB92) concentration during the time under visible light. Effects of pH, dye concentration, photocatalyst dosage, and different scavengers on photocatalytic performance were explored. Maximum photocatalytic degradation was observed at pH = 7. Among different scavengers, silver nitrate demonstrated the maximum activity for dye degradation. Photocatalyst with 400 ppm concentration showed the highest activity. Proposed mechanism and reaction kinetics were also discussed.

Keywords: Nanocomposites, Photocatalytic activity, Graphitic carbon nitride, Organic pollutant

INTRODUCTION

Photocatalytic processes offer effective and important strategy for pollutant elimination, clean hydrogen production and some material preparation [1-8]. Three main classes of photocatalysts have been used for these purposes. Transition metal oxides such as TiO_2 and ZnO which are stable and low cost. Because of wide band gap their energy conversion efficiency is low. The second class of photocatalysts are chalcogenides (CdS and CdSe) [2]. The photocorrosion is the main disadvantage of these materials. Metal Organic frameworks as third part of this classification have attracted attention due to high surface area and pore volume. MOF(5) in the photodegradation of phenol firstly was investigated in 2007 [3].

Among different photocatalysts, graphitic carbon nitride (g-C_3N_4) has recently transpired as an ideal material with good visible light response and thermal and chemical stability [9]. Graphitic carbon nitride has a band gap about 2.7 eV causing this metal free material has good performance in water splitting and organic pollutant degradation [10]. There are some restrictions for this photocatalysts limiting its application drastically. Low electronic conductivity and quantum efficiency, fast electron-hole recombination and weak redox ability of electron and hole are some important limitations of g-C_3N_4 [10-12]. There are some methods to overcome problems and improve photocatalytic activity; doping of different elements, heterojunction preparation, morphology control, *etc.* [10]. Fabrication of heterostructures not only reduces the electron-hole recombination, but also by synergistic effects of other semiconductors leads to novel material production with special properties.

Graphitic carbon nitride could be prepared by several methods. Pyrolysis of urea, dicyanidamine, melamine and thiourea are well known and facile methods to reach g-C_3N_4 [9-12]. The g-C_3N_4 bulk could be exfoliated to sheets by hydrothermal method, sonication, heating and acid treatment [13]. The g-C_3N_4 sheets having higher surface area and active edges could be dispersed easily in water and other solvents. Silver oxide (Ag_2O) with lattice parameter of 0.472 nm and band gap energy of 1.2 eV and energy level

*Corresponding author. E-mail: gholami@sharif.edu

of CB edge of 0.2 eV is widely used in catalyst, cleaning and electrode industries [14-15]. Ag_2O is very photosensitive and usually is not stable enough. Hence, researchers prefer use Ag_2O as a cocatalyst in heterostructures. On the other hand, Ag_2O can be used as sensitizer to tune the light response to visible region. Graphitic carbon nitride could fabricate a p-n junction by coupling with a p-type semiconductor like Ag_2O [15]. In this situation photogenerated electron and hole transfer effectively midst the lattice. The efficiency of silver oxide coupling photocatalysts is dependent to particle size and weight percentage of Ag_2O. Large amount of noble metals like silver limits its environmental applications. Hence, control of Ag_2O size in photocatalytic application plays an important role to reach maximum efficiency. Now, preparation of silver containing photocatalysts in big scale is a challenge [15]. Graphene and graphene oxide with desirable and unique properties, have opened up new academic and industries fields in last decade [9]. The research performed approved that graphene could enhance the photocatalytic activity if it is joint chemically and electronically to other structures [16]. Graphene oxide and graphene are able to effectively adsorb organic molecules on the photocatalyst surface through π-π interactions.

Loading of graphene on photocatalysts is an effective way to improve the photocatalytic activity and stability [17-22]. Furthermore, hybridization of silver oxide with graphene could reduce the electron-hole recombination. The aim of this work is to synthesize, and subsequently characterization and photocatalytic activity investigation of g-C_3N_4/reduced graphene oxide/Ag_2O nanostructures. Photocatalytic degradation of methylene blue (MB) and kinetics of degradation reaction are also studied.

EXPERIMENT

Photocatalyst Synthesis

Direct pyrolysis of melamine was used for g-C_3N_4 production [23]. 20 g of melamine was placed in a semi closed crucible and heated to 550 °C at static air at a ramp rate of 2.5 degree min^{-1}. The crucible kept for 4 h at this temperature and finally the product was cooled to the room temperature. The obtained yellow product grounded in to a fine powder. Graphene oxide was synthesized with modified Hummers' method [24]. 1 g of fine pure graphite powder and 0.5 g of sodium nitrate was added to 24 ml of concentration sulfuric acid in an ice bath. After 2 h vigorous stirring, 3 g potassium permanganate was added slowly to mixture. 30 ml of DI water was added and the mixture was stirred for 24 h. The color of mixture in this stage was brown. 3.5 ml of H_2O_2 (30% w/w) was added dropwise and mixture was stirred 4 h at room temperature. The residual sediment was washed several times with dilute HCl solution and black product was dried in an oven over a night at 80 °C. For preparation of the reduced graphene oxide, 100 mg of graphene oxide powder was added to 100 ml of DI water and mixture was sonicated for 2 h. Then, 20 ml hydrazine was added and mixture was refluxed at 70 °C for 2 h. To synthesize g-C_3N_4/reduced graphene oxide/Ag_2O, 15 mg of the reduced graphene oxide was sonicated in 20 ml DI water, and then, 0.5 g of sodium hydroxide was added to it and stirred for 3 h. In another vessel, 0.03 g of g-C_3N_4 powder and 30 ml of DI water were sonicated for 1 h, and 0.2 g of $AgNO_3$ in 1 ml of concentrated ammonia was added into the mixture and stirred for 1 h. The pH of solution was adjusted to 7.5 by dilute HNO_3 adding. Second mixture was added slowly to the first mixture and stirred for 12 h. The final product was separated by filtration and washed three times with water and ethanol and dried in oven at 80 °C for 15 h.

Apparatus

AB92 absorption was scanned by UV-Vis spectrophotometer (GBC Cintra 40). The morphology of the photocatalyst surface was investigated by scanning electron microscope (SEM, KYKY-EM3200). Transmission electron microscopy (TEM, Philips Tecnai G220, operated at 120 kV) was applied to specify the mean average size of nanoparticles. X-ray diffraction (XRD) patterns of materials were recorded on a Bruker D8 advance X-ray diffractometer with Cu K_a irradiation.

Photocatalytic Experiment

The experiment was performed in a glass batchscale reactor. Osram 125W lamp was used as light source. The lamp was located at 10 cm top of the reactor. The incident photon flux entering the photoreactor was varied from 1.11×10^{-6} to 2.13×10^{-6} einstein cm^{-2} s^{-1}. The reactor

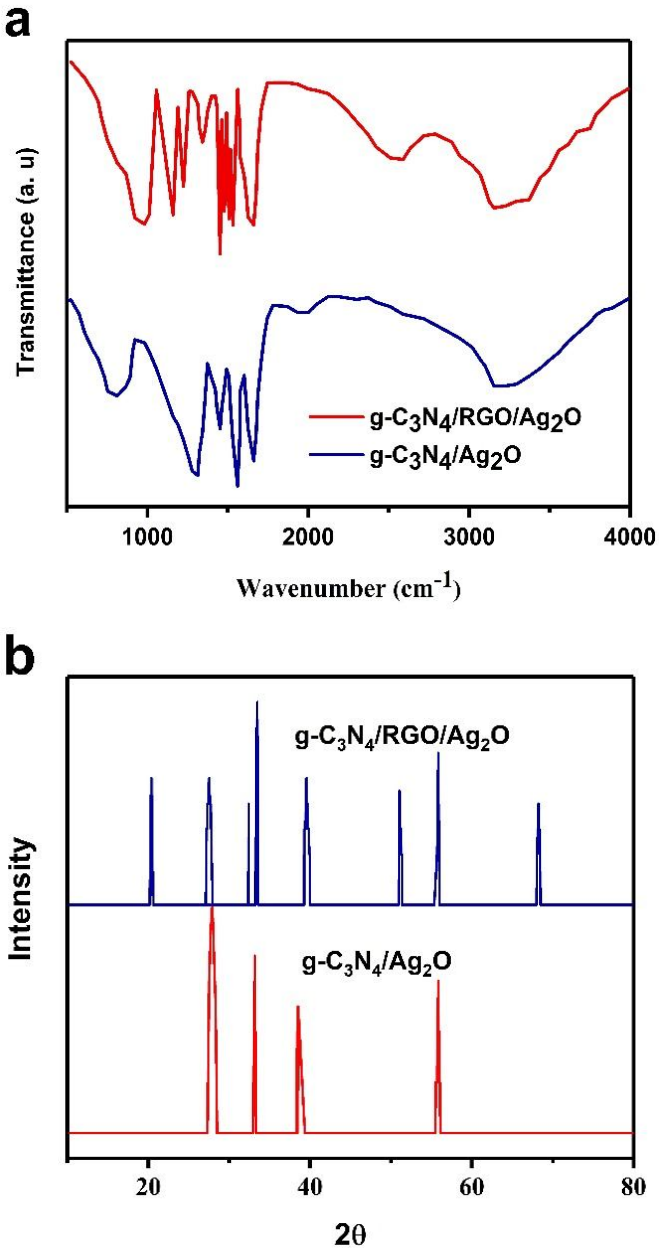

Fig. 1. IR spectra (a), and XRD patterns (b) of the prepared samples.

temperature was controlled by water circulation in outer wall of reactor. The photocatalytic activity was investigated by scanning the AB92 concentration *via* UV-Vis spectrophotometer. For each experiment, the photocatalysts were removed from the mixture by centrifuge, and the AB92 concentration was analyzed in maximum absorption wavelength of AB92. AB92 solution was prepared in different concentrations in DI water and an appropriate amount of AB92 solution, and determined photocatalysts dosage transferred to photoreactor and mixture stirred by a magnet. At the beginning of the experiment, a suspension containing 400 ppm of photocatalyst and 50 ml of AB92 solution was prepared and stirred in photoreactor for 45 min in dark to reach

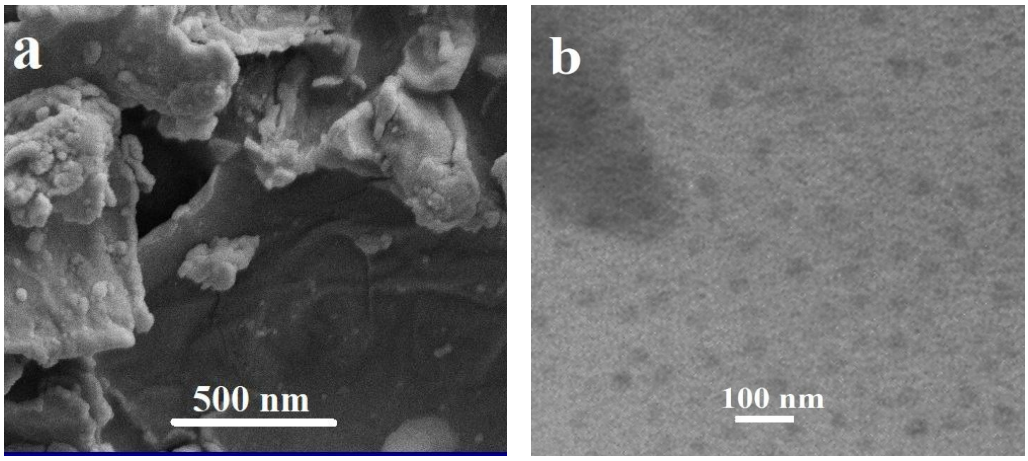

Fig. 2. SEM image of g-C_3N_4/RGO/Ag_2O (a), and TEM image of nanoparticles (b).

equilibrium.

RESULTS AND DISCUSSION

FT-IR spectra of g-C_3N_4/Ag_2O and g-C_3N_4/RGO/Ag_2O are presented in Fig. 1a. Characteristic absorption peaks of C_3N_4 could be observed in g-C_3N_4/Ag_2O and g-C_3N_4/RGO/Ag_2O. The broad band at 3000-3700 cm^{-1} is related to N-H stretching vibration of C_3N_4 structure, and O-H stretching vibration of H_2O which could physically adsorb on materials surface. The strong bonds at 1300, 1400 and 1550 cm^{-1} are corresponded to C=N and C-N stretching vibration [25]. The peak at 1600 cm^{-1} is attributed to C=C group in C_3N_4/RGO/Ag_2O [26]. Figure 1b demonstrates the smoothed XRD patterns of g-C_3N_4/Ag_2O and g-C_3N_4/RGO/Ag_2O. Pronounced peak in 27.4° is indexed to {002} diffraction plane of graphite like carbon nitride (JCPDS 87-1526). Because of stacking distance in conjugated aromatic system, this peak appeared. When Ag_2O is coupled with C_3N_4 and Graphene some new strong peaks are observed. Characteristic diffraction peaks of Ag_2O are at 32.8, 38, 55 and 68.7 (JCPDS 41-1104).

The layered, laminated structure of g-C_3N_4/RGO/Ag_2O is shown in Fig. 2a. As can be seen, silver oxide nanoparticles with mean average size of 50 nm have been dispersed uniformly on the reduced graphene oxide sheets (TEM image in Fig. 2b). Optical properties of g-C_3N_4/Ag_2O and g-C_3N_4/RGO/Ag_2O were investigated by UV-Vis diffuse absorption spectra. Figure 3a illustrates the absorption spectra of g-C_3N_4/Ag_2O and g-C_3N_4/RGO/Ag_2O structures. According to 2.7 eV band gap of C_3N_4, the absorption edge of pure C_3N_4 should be about 450 nm [10]. This is originated from charge transfer of valance band (N2p electrons) to conduction band orbitals (formed by C2p orbitals). By coupling of Ag_2O with C_3N_4 and charge transfer transition between Ag_2O and C_3N_4, the optical absorption of structure increases in visible region. Furthermore, the results of UV-Vis DRS investigations implied that for g-C_3N_4/RGO/Ag_2O the optical absorption has increased to some extent. Semiconductor band gap energy can be determined by Tauc/David-Matt models explained according to Eq. (1):

$$(Ah\upsilon) = a(h\upsilon - E_g)^{n/2} \quad (1)$$

where a is absorption coefficient, h is plank's constant, υ is light frequency and E_g is semiconductor band gap, and A is a constant. The value of n is dependent of transition type and directly/indirectly allowed transition (n = 1 for direct transition and n = 4 for indirect transition). By drawing the plot of $(ah\upsilon)^2$ *versus* hυ (Fig. 3b), the band gap of g-C_3N_4/Ag_2O and g-C_3N_4/RGO/Ag_2O appeared at about 2.61 and 2.5 eV, respectively.

Dye degradation kinetics in most cases obeys from Langmuir-Hinshelwood kinetic model represented in Eq. (2) [7,27-29].

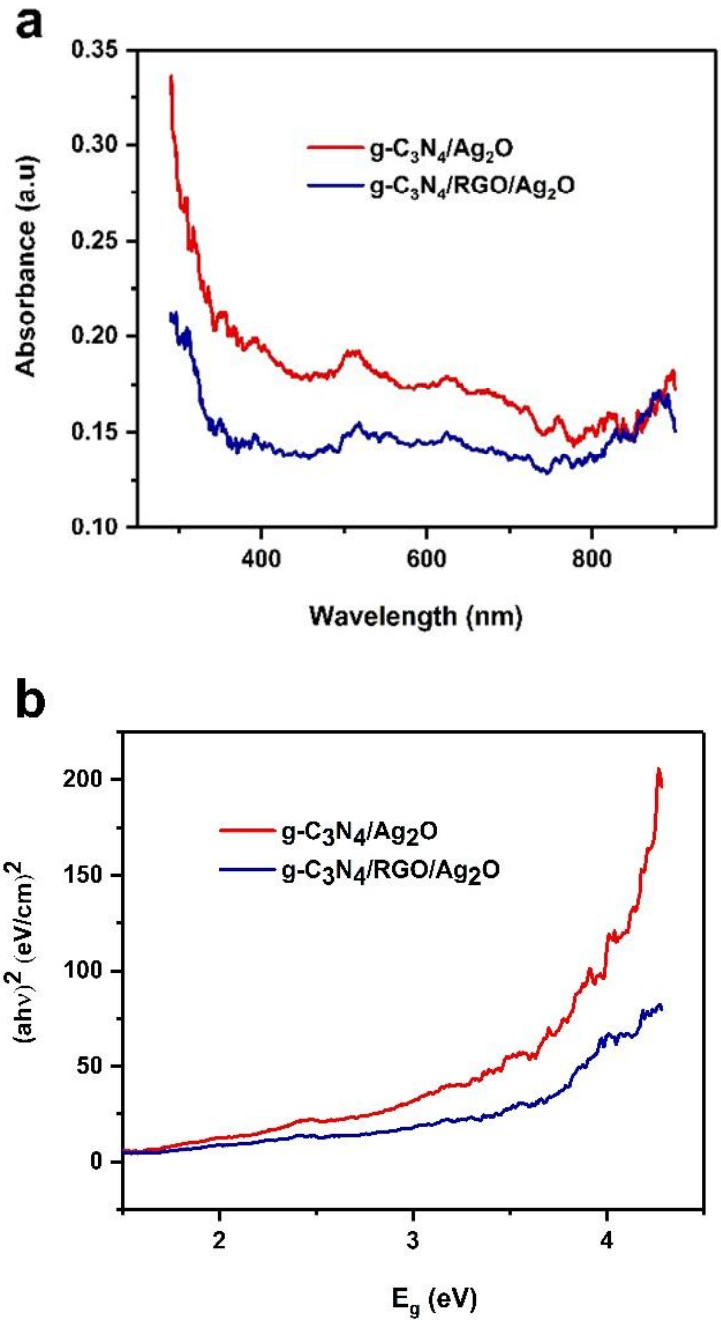

Fig. 3. Absorption spectra (a), and band gap energy (b) of the prepared samples.

$$R = dC/dt = kK/1 + kC \quad (2)$$

$$\ln C_o/C = kKt = k_{app}t \quad (3)$$

In low dye concentration, Eq. (2) could change to a pseudo first order equation. The rate constant (k_{app}) can be calculated by Eq. (3).

In Fig. 4, the linear plot of $\ln C_o/C$ *vs*. t approved the pseudo first order equation. The rate constant for g-C_3N_4/RGO/Ag_2O was 0.0383 min^{-1}. In heterogeneous

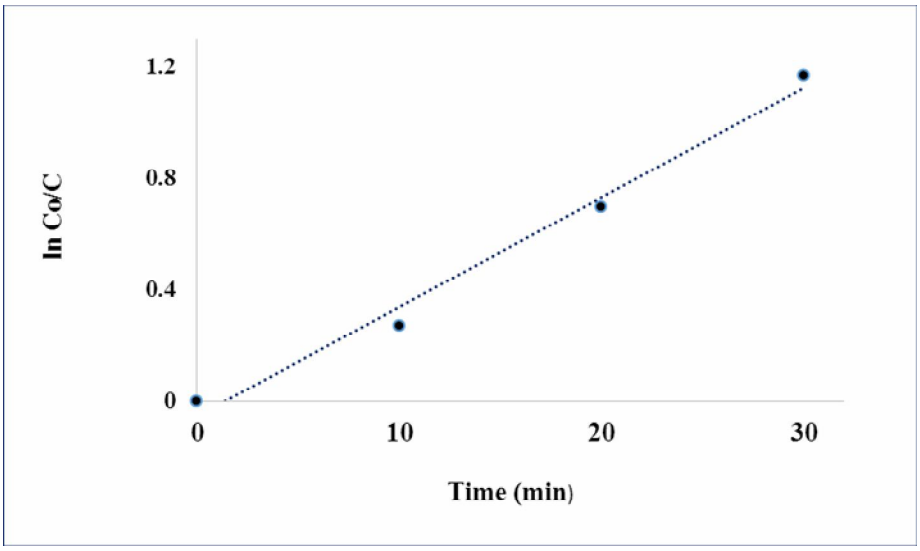

Fig. 4. First order reaction. [Catal] = 400 ppm, [dye] = 20 ppm, pH = 7.

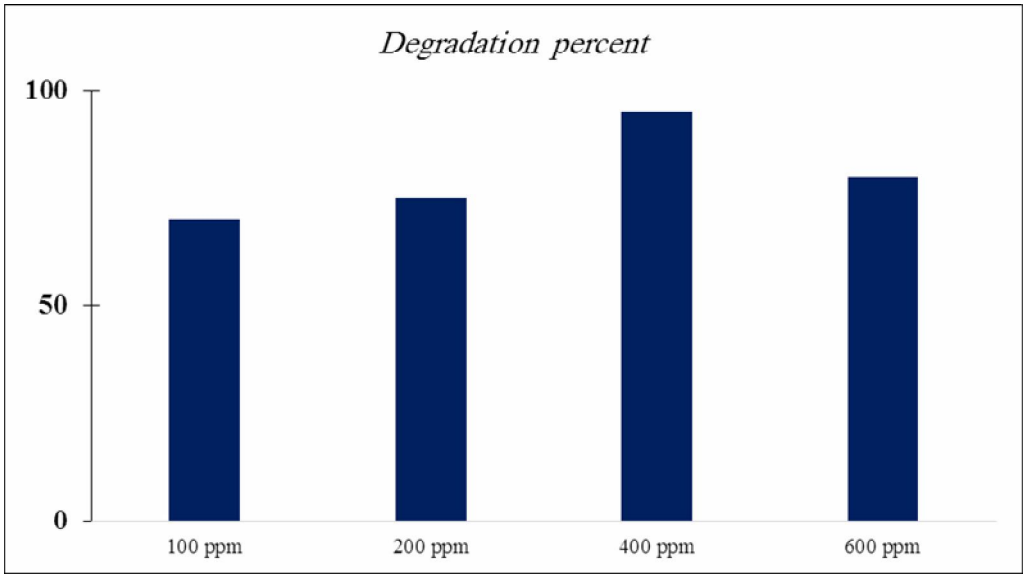

Fig. 5. Effect of photocatalyst dosage on dye degradation. [dye] = 20 ppm, pH = 7, time = 30 min.

reactions the reaction rate directly is related to catalysts dosage. As illustrated in Fig. 5, by increasing the catalyst dosage from 100 ppm to 400 ppm the degradation percentage is elevated. In concentration over 600 ppm, the photocatalytic activity deceased because of light reflection of nanostructures in mixture [30]. Sticking of particles in catalyst high concentration could be another reason for this phenomena.

Figure 6 shows the dye concentration effect on photocatalytic activity. As can be seen, by increasing the dye concentration from 10 ppm to 30 ppm, the dye adsorption and degradation are decreased. High initial dye

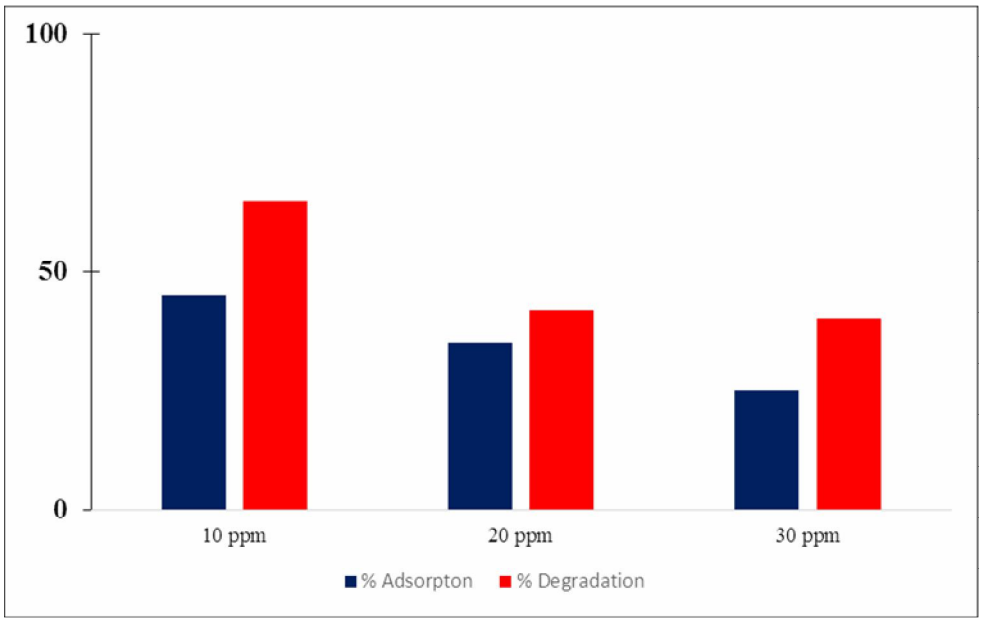

Fig. 6. Effect of AB92 concentration on dye degradation. [catal] = 200 ppm, pH = 7, time = 30 min.

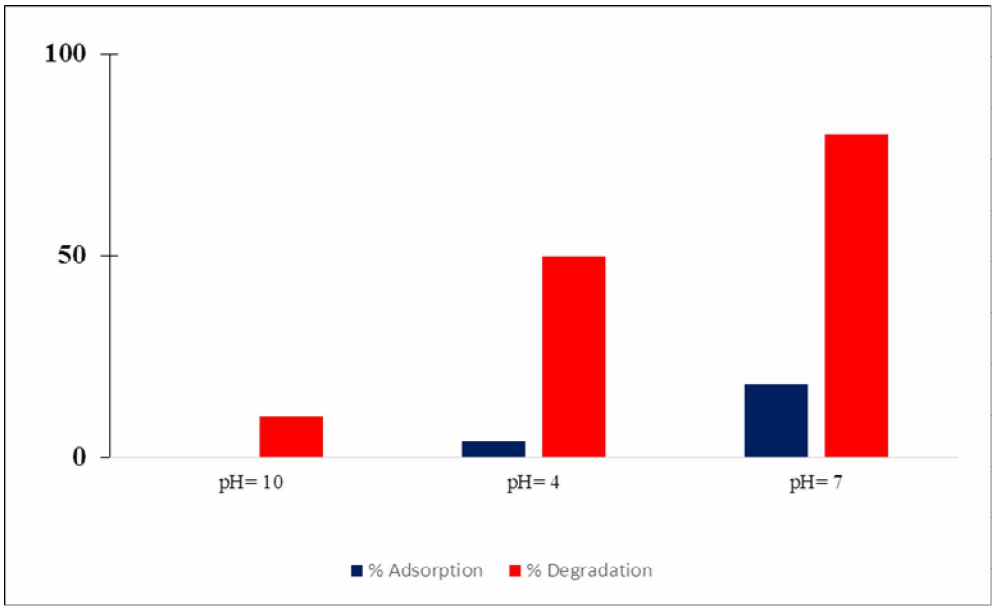

Fig. 7. Effect of pH on dye degradation. [dye] = 20 ppm, [catal] = 200 ppm, time = 30 min.

concentration could affect the light penetration trough the solution. When the light penetration is declined, less photons reach the photocatalyst surface [31]. Hence, dye molecules and photocatalyst surface compete for light absorption. There are many reports implied that dye degradation is limited by intermediate produced during the

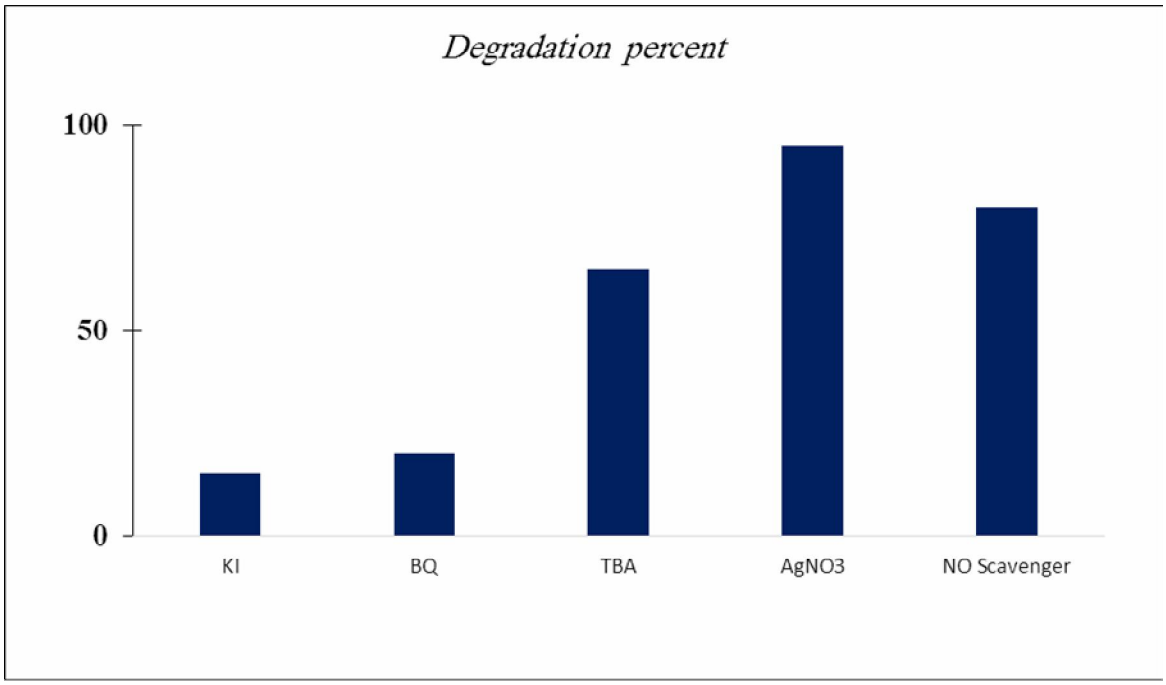

Fig. 7. Effect of different scavenger (0.003 mmol) on dye degradation. [dye] = 20 ppm, [catal] = 200 ppm, time = 30 min, pH = 7.

photoprocesses [32,33]. If the dye concentration increases, the intermediate content is elevated. In this condition, the adsorption competition on photocatalyst surface is amplified between dye and intermediate. Important part of photocatalytic reaction takes placed in region near the light irradiation called reaction zone. When the concentration of dye enhances, because of delay in light penetration, the dye degradation occurs far from the reaction zone. The effect of pH on the photocatalytic activity of g-C_3N_4/RGO/Ag_2O has been investigated that is demonstrated in Fig. 7. Three different pHs were selected and maximum activity was observed in neutral pH. Initial pH is an important parameter for controlling the process. Initial pH not only affects the dye adsorption on photocatalyst surface but also alters the photocatalytic redox process. In acidic media, the surface charge becomes positive that drastically repulses the dye molecules. When the pH increases to basic environment, the surface charge becomes negative reducing the hydroxyl radical formation and photo-oxidation efficiency [34]. As can be seen in Fig. 7, the adsorption of dye in pH = 7 is more than that of other pHs that accelerates the photocatalytic activity. When light is irradiated to photocatalyst surface, the electron is transferred from valance band of g-C_3N_4 to conduction band. Conduction band of g-C_3N_4 is negative compared to conduction band of Ag_2O and electrons can move to Ag_2O conduction band. Oxygen molecule adsorbed on Ag_2O surface is reduced to oxygen radicals and similar phenomena could take place on graphene surface. Oxygen radicals by reactions with H^+ can produce another intermediate. (Eqs. (4)-(10)). Furthermore, hole could directly degrade AB 92 by its strong oxidative ability.

$$\text{Photocatalyst} + h\upsilon \longrightarrow e^- + h^+ \quad (4)$$

$$Ag_2O + H_2O + 2e^- \longrightarrow 2Ag + 2OH^- \quad (5)$$

$$RGO(e^-) + O_2 \longrightarrow RGO + O_2^{\cdot-} \quad (6)$$

$$O_2^{\cdot-} + H^+ \longrightarrow {}^{\cdot}OOH \quad (7)$$

$$HO_2^{\cdot} + H^+ \longrightarrow H_2O_2 \quad (8)$$

$$H_2O_2 + e^- \longrightarrow {}^{\cdot}OH + OH^- \quad (9)$$

$h^+, O_2^{-\cdot}, OH^{\cdot} + AB92 \longrightarrow$ degradation products (10)

Graphene has high surface area and by providing site in photocatalyst enhances the dye adsorption which finally increases the photo degradation. Graphene as an ideal electron acceptor could take the electrons. Fast electron transfer in graphene takes place because of graphene π conjugated structure. Graphene in g-C_3N_4/RGO/Ag_2O heterostructure could prevent electron-hole recombination and accelerate the photocatalyst activity. Graphene decreases the Ag^+ reduction to Ag during photocatalytic process and helps photocatalyst becomes stable in more time [35].

By using different scavenger, the effective species could be determined in photocatalytic reaction. Generally accepted that electron-hole produced in conduction band and valance band causes photocatalytic activity. Electron and hole can interact by adsorbed O_2, H_2O and OH^- on photocatalyst surface and produce secondary active species (Eqs. (6)-(9)). To study the role of each species in photocatalytic reactions and find out the detailed mechanism using scavenger is necessary. Four different types of scavengers were applied in this work. The results are presented in Fig. 8. Potassium iodide reduced the activity to some extent. KI as a hole and $OH^{\cdot}$ scavenger takes out the holes from photcatalyst surface and decreases the dye degradation. This result shows that hole has the maximum effect on dye degradation (Eqs. (11)-(16)).

$$I^- \longrightarrow I^{\cdot} + e^- \quad (11)$$

$$I^- + I^{\cdot} \longrightarrow I_2^{-\cdot} \quad (12)$$

$$I_2^{-\cdot} \longrightarrow I_2 + e^- \quad (13)$$

$$I^- + OH^{\cdot} \longrightarrow OH^- + I^{\cdot} \quad (14)$$

$$I_2 + OH^{\cdot} \longrightarrow HOI + I^{\cdot} \quad (15)$$

$$I^- + I^{\cdot} \longrightarrow I_2^{-\cdot} \quad (16)$$

Para benzoquinone (BQ) has an impressive effect on dye degradation implying that oxygen radicals have important role in reaction mechanism. Tert-butyl alcohol (TBA) has weaker effect compared to BQ and KI. TBA is an $OH^{\cdot}$ scavenger that could be effective in reaction extent. $AgNO_3$ is an electron scavenger. High photocatalytic activity in the presence of $AgNO_3$ causes that electrons have no effects on photodegradation. Furthermore, by taking out the electrons from reaction media, the electron-hole recombination is inhibited. Hence, holes could effectively play positive role and degrade AB92.

CONCLUSIONS

g-C_3N_4/Ag_2O and g-C_3N_4/RGO/Ag_2O were synthesized and characterized by different methods. Photocatalytic activity was investigated by monitoring the AB92 concentration change during the reaction. On the basis of the results, by increasing the dye concentration, the photocatalytic activity decreases. Photocatalyst dosage to determined elevating could increase the dye degradation. In pH = 7 maximum photocatalytic efficiency wsa observed. Using different scavengers approved that the kinetics of reaction is first order and holes in reaction media have the most important role in dye degradation.

ACKNOWLEDGEMENTS

This work was supported by the Iran National Science Foundation [grant number 97002729].

REFERENCES

[1] Zhang, K.; Guo, L., Metal sulphide semiconductors for photocatalytic hydrogen production, *Catal. Sci. Technol.* **2013**, *3*, 1672-1690, DOI: 10.1039/C3CY00018D.

[2] Tran, P. D.; Wong, L. H.; Barber, J.; Loo, J. S. C., Recent advances in hybrid photocatalysts for solar fuel production, *Energy Environ. Sci.* **2012**, *5*, 5902-5918. DOI: 10.1039/C2EE02849B.

[3] Alvaro, M.; Carbonell, E.; Ferrer, B.; Xamena FX, L. I.; Garcia, H., Semiconductor behavior of a metal-organic framework (MOF), *Chem.-A Europ. J.,* **2007**, *13*, 5106-5112. DOI: 10.1002/

chem.200601003.

[4] Habibi-Yangjeh, A.; Golzad-Nonakaran, B., Fabrication of magnetically recoverable nanocomposites by combination of Fe_3O_4/ZnO with AgI and Ag_2CO_3: Substantially enhanced photocatalytic activity under visible light, *Phys. Chem. Res.,* **2018**, *6*, 415-431. DOI: 10.22036/pcr.2018.116937.1461.

[5] Esfandfard, S. M.; Elahifard, M. R.; Behjatmanesh-Ardakani, R.; Kargar H., DFT study on oxygen-vacancy stability in rutile/anatase TiO_2: Effect of cationic substitutions, *Phys. Chem. Res.,* **2018**, *6*, 547-563. DOI: 10.22036/PCR.2018.128713.1481

[6] Padervand, M.; Salari, H.; Ahmadvand, S. S.; Gholami, M. R., Removal of an organic pollutant from waste water by photocatalytic behavior of AgX/TiO_2 loaded on mordenite nanocrystals, *Res. Chem. Intermed,* **2012**, *38*, 1975-1985. DOI: 10.1007/s11164-012-0519-8.

[7] Salari, H.; Khasevani, S. G.; Setayesh, S. R.; Gholami, M. R., Enhanced visible light photocatalytic activity of nano-BiOCl/$BiVO_4$/Zeolite pn heterojunction and Ag/BiOCl/$BiVO_4$ hybrid, *Mater. Res. Innov,* **2018**, *22*, 137-143. DOI: 10.1080/14328917.2016.1264849.

[8] Padervand, M.; Vossoughi, M.; Yousefi, H.; Salari, H.; Gholami, M. R., An experimental and theoretical study on the structure and photoactivity of XFe_2O_4 (X = Mn, Fe, Ni Co, and Zn) structures, *Russ. J. Phys. Chem. A,* **2014**, *88*, 2451-2461. DOI: 10.1134/S0036024414130184.

[9] Shabani Shayeh, J.; Salari, H.; Daliri, A.; Omidi, M.; Decorative reduced graphene oxide/C_3N_4/Ag_2O/ conductive polymer as a high performance material for electrochemical capacitors, *Appl. Surf. Sci.,* **2018**, *447*, 374-380. DOI: 10.1016/j.apsusc.2018.03.249.

[10] Xu, M.; Han, L.; Dong, S., Facile fabrication of highly efficient g-C_3N_4/Ag_2O heterostructured photocatalysts with enhanced visible-light photocatalytic activity, *Appl. Mater. Interfaces,* **2013**, *5*, 12533-12540. DOI: 10.1021/am4038307.

[11] Yin, R.; Luo, Q.; Wang, D.; Sun, H.; Li, Y.; Li, X.; An, J., SnO_2/g-C_3N_4 photocatalyst with enhanced visible-light photocatalytic activity, *J. Mater. Sci.*, **2014**, *49*, 6067-6073. DOI: 10.1007/s10853-014-8330-0.

[12] Wan, Z.; Zhang, G.; Wu, X.; Yin, S., Novel visible-light-driven Z-scheme $Bi_{12}GeO_{20}$/g-C_3N_4 photocatalyst: Oxygen-induced pathway of organic pollutants degradation and proton assisted electron transfer mechanism of Cr(VI) reduction, *Applied Catalysis B: Environmental,* **2017**, *207*, 17-26. DOI: 10.1016/j.apcatb.2017.02.014.

[13] Yang, Y.; Geng, L.; Guo, Y.; Meng, J.; Guo, Y.; Easy dispersion and excellent visible-light photocatalytic activity of the ultrathin urea-derived g-C_3N_4 nanosheets, *Appl. Surf. Sci.*, **2017**, *425*, 535-546. DOI: 10.1016/j.apsusc.2017.06.323.

[14] Wang, X.; Li, S.; Yu, H.; Yu, J.; Liu, S.; Ag_2O as a new visible-light photocatalyst: Self-stability and high photocatalytic activity, *Chem. Eur. J.,* **2011**, *17*, 7777-7780. DOI: 10.1002/chem.201101032.

[15] Dinh, C. T.; Nguyen, T. D.; Kleitz, F.; Do, T. O., Large-scale synthesis of uniform silver orthophosphate colloidal nanocrystals exhibiting high visible light photocatalytic activity, *Chem. Commun*. **2011**, *47*, 7797-7799. DOI: 10.1039/C1CC12014J.

[16] Ji, Z.; Shen, X.; Yang, J,; Xu, Y.; Zhu, G.; Chen, K., Graphene oxide modified Ag_2O nanocomposites with enhanced photocatalytic activity under visible-light irradiation, *Eur. J. Inorg. Chem.,* **2013**, 6119-6125. DOI:10.1002/ejic.201301105.

[17] Ma, X.; Xiang, Q.; Liao, Y.; Wen, T.; Zhang, H., Visible-light-driven CdSe quantum dots/graphene/ TiO_2 nanosheets composite with excellent photocatalytic activity for E. coli disinfection and organic pollutant degradation, *Applied Surface Science,* **2018**, *457*, 846-855. DOI: 10.1016/j.apsusc.2018.07.003.

[18] Wu, X.; Chen, F.; Wang, X.; Yu, H., *In situ* one-step hydrothermal synthesis of oxygen-containing groups-modified g-C_3N_4 for the improved

photocatalytic H2-evolution performance, *Appl. Surf. Sci.,* **2018**, *427*, 645-653. DOI: 10.1016/ j.apsusc.2017.08.050.

[19] Cheng, F.; Yin, H.; Xiang, Q., Low-temperature solid-state preparation of ternary CdS/g-C_3N_4/CuS nanocomposites for enhanced visible-light photocatalytic H_2-production activity, *Appl. Surf. Sci.,* **2017**, *391*, 432-439. DOI: 10.1016/ j.apsusc.2016.06.169.

[20] Lang, Di.; Shen, T.; Xiang, Q., Roles of MoS_2 and graphene as cocatalysts in the enhanced visible-light photocatalytic H_2 production activity of multiarmed CdS nanorods, *Chem. Cat. Chem.,* **2015**, *7*, 943-949. DOI: 10.1002/cctc.201403062.

[21] Xu, Y.; Mo, Y.; Tian, J.; Wang, P.; Yu, H.; Yu, J., The synergistic effect of graphitic N and pyrrolic N for the enhanced photocatalytic performance of nitrogen-doped graphene/TiO_2 nanocomposites, *Appl. Catal. B: Environ*., **2016**, *181*, 810-817. DOI: 10.1016/j.apcatb.2015.08.049.

[22] Cheng, L.; Xiang, Q.; Liao, Y.; Zhang, H., CdS-based photocatalysts, *Energy Environ. Sci.,* **2018**, *11*, 1362-1391. DOI: 10.1039/C7EE03640J.

[23] Ma, D.; Wu, J.; Gao, M.; Xin, Y.; Ma, T.; & Sun, Y.; Fabrication of Z-scheme g-C_3N_4/RGO/Bi_2WO_6 photocatalyst with enhanced visible-light photocatalytic activity. *Chem. Engin. J.* **2016**, *290*, 136-146. DOI: 10.1021/ acs.iecr.7b01840.

[24] Chen, Q.; Zhao, Y.; Huang, X.; Chen, N.; & Qu, L., Three-dimensional graphitic carbon nitride functionalized graphene-based high-performance supercapacitors. *J. Mater. Chem. A*. **2015**, *3*, 6761-6766. DOI: 10.1039/C5TA00734H.

[25] Yan, H.; Yang, H., TiO_2-g-C_3N_4 composite materials for photocatalytic H2 evolution under visible light irradiation. *J. Alloys and Compounds,* **2011**, *509*, 26-29. DOI: 10.1016/j.jallcom.2010.09.201.

[26] Si, Y.; Samulski, E. T., Synthesis of water soluble graphene. *Nano Lett.,* **2008**, *8*, 1679-1682. DOI: 10.1021/nl080604h.

[27] Padervand, M.; Salari, H.; Sadeghzadeh Darabi, F.; Khodadadi Moghaddam, M.; Gholami, M. R., Photocatalytic reduction of nitrobenzene with $NaBH_4$ in aqueous medium over the Ag/AgBr/TiO_2/ NZ and Ag/AgBr/NZ Nanocomposites, *Int. J. Mater. Chem.,* **2011**, *1*, 49-57. DOI: 10.5923/ j.ijmc.20110101.02.

[28] Salari, H.; Hallett, J. P.; Padervand, M.; Gholami, M. R., Systems designed with an ionic liquid and molecular solvents to investigate the kinetics of an SNAr reaction, *Progress in Reaction Kinetics and Mechanism*, **2013**, *38*, 157-170. DOI: 10.3184/ 146867813X13632857557572.

[29] Salari. H.; Rohani, H.; Elahifard, M. R.; Hosseini, M.; Gholami, M. R., Solvents design on the basis of molecular-microscopic properties of binary mixtures for lycopene extraction, *Am. J. Chem.,* **2012**, *2*, 94-98. DOI: 10.5923/j.chemistry.20120202.14.

[30] Hu, L.; Chen, F.; Hu, P.; Zou, L.; & Hu, X., Hydrothermal synthesis of SnO_2/ZnS nanocomposite as a photocatalyst for degradation of Rhodamine B under simulated and natural sunlight. *J. Mol. Catal. A: Chem.* **2016**, *411*, 203-213. DOI: 10.1016/ j.molcata.2015.10.003.

[31] Yang, Q.; Chen, F.; Li, X.; Wang, D.; Zhong, Y.; Zeng, G., Self-assembly Z-scheme heterostructured photocatalyst of Ag_2O@Ag-modified bismuth vanadate for efficient photocatalytic degradation of single and dual organic pollutants under visible light irradiation. *RSC Adv.* **2016**, *6*, 60291-60307. DOI: 10.1039/C6RA04862E.

[32] Rezaei, M.; Habibi-Yangjeh, A., Simple and large scale refluxing method for preparation of Ce-doped ZnO nanostructures as highly efficient photocatalyst, *Appl. Surf. Sci.,* **2013**, *265*, 591-596. DOI: 10.1016/ j.apsusc.2012.11.053.

[33] Wang, H.; Yuan, X.; Z.; Wu, Y.; Zeng, G. M.; Chen, X. H.; Leng, L. J.; Li, H., Synthesis and applications of novel graphitic carbon nitride/metal-organic frameworks mesoporous photocatalyst for dyes removal, *Appl. Catal., B,* **2015**, *174*, 445-454. DOI: 10.1016/j.apcatb.2015.03.037.

[34] Mart´ınez-de la Cruz, A.; P´erez, U. G., Photocatalytic properties of $BiVO_4$ prepared by the

co-precipitation method: degradation of rhodamine B and possible reaction mechanisms under visible irradiation, *Mater. Res. Bull.,* **2010**, *45*, 135-141. DOI: 10.1016/j.materresbull.2009.09.029.

[35] Chai, B.; Li, J.; Xu, Q., Reduced grapheme oxide grafted Ag_3PO_4 composites with efficient photocatalytic activity under visible-light irradiation. *Indust. Engin. Chem. Res.* **2014**, 53, 8744-8752. DOI: 10.1021/ie4041065.